APRIL 1982

LIDS-FR-1206

MASSACHUSETTS INSTITUTE OF TECHNOLOGY
LABORATORY FOR INFORMATION AND DECISION SYSTEMS
CAMBRIDGE, MASSACHUSETTS 02139

FINAL REPORT ON

HYBRID OPERATOR MODELS FOR DIGITALLY-
IMPLEMENTED CONTROL SYSTEMS

by

Gunter Stein
Michael Athans
Peter Thompson

Submitted to: Mr. Jarrell R. Elliot
                 Mail Stop 152-A
                 Theoretical Mechanics Branch
                 NASA Langley Research Center
                 Hampton, Virginia   22365

TABLE OF CONTENTS

1. INTRODUCTION AND SUMMARY

Background

Over the past several years, MIT's Laboratory for Information and Decision Systems (LIDS) has been conducting research for NASA on the properties of multivariable digital control systems [1]. These types of systems are becoming increasingly important as small, powerful, flight-qualified digital computers take over the burden of control law implementation in various NASA vehicles and other control system applications. Examples include the shuttle orbiter, the HIMAT and F-8C DFBW aircraft, satellites and space probes such as Viking and Galileo, various proposed large space systems, and many more.

The overall goal of the research program has been to evolve improved design methods for multivariable sample-data control laws. Research effort was concentrated initially on the primary available synthesis tool--namely the sample-data (discrete-time) Linear-Quadratic (LQ) regulator problem [Athans, 2]. Various properties of this problem formulation were studied, and key features of its solution were investigated. In the latter category, the basic "robustness properties" (e.g. multivariable gain margins and phase margins) of sample-data LQ solutions received particular emphasis.

Two major conclusions emerged from these initial studies. First, the sample-data LQ problem, like other sample-data synthesis formulations suffers from the over idealized time sequence representation of the control process. The process is described only "at the sampling instant," with no information about intersample behavior or intersample control requirements

other than what can be predicted from values of states and controls at
the sampling times [Levis, 3]. The need for devices such as prefilters
(which appear in virtually every practical digital control implementation)
and the potential benefits of higher-order hold devices cannot be addressed
within this pure sample-data framework.

The second major finding concerns the robustness properties of
sample-data LQ control systems. These turn out to be fundamentally inferior
to their continuous-time counterparts. Recall that the latter enjoy impres-
sive uncertainty tolerances including -6db to + ∞db gain margin or ±60deg
phase margin in all combinations of control channels [Safonov and Athans, 4].
These margins are guaranteed for every continuous-time LQ design, inde-
pendent of specific plant or cost function parameter values. In the sample-
data case, the corresponding uncertainty margins are generally less than
the ranges above and are functions of specific plant and cost function values.
Hence, no a-priori robustness guarantees can be stated for sample-data LQ
control laws [Safonov, 5].

Motivated by these two apparent limitations of the existing LQ
synthesis methodology, the research effort was re-directed toward more
fundamental issues of digitally implemented control systems. The first task
of the redirected effort was to find a mathematical representation which
properly captures both the continuous-time (analog) and the discrete-time
(digital) processes which occur simultaneously in a digital control system.
Such a representation was developed and is called the "hybrid operator model"
of the control process. This model provides an analog input-output view of the

control process which explicitly includes sampling operations, digital calculations, hold operations, and continuous plant evolutions. The structure of this operator is summarized briefly in Section 2 below and in more detail in a Master's thesis by A. Kostovetzky [6].

An immediate application of the hybrid operator is to explain the common use of prefilters in practical digital control systems. Simple norm calculations in [6] show that the hybrid operator has unbounded gain (in an appropriate function space sense) as the sampling process tends toward the ideal impulsive sampling normally assumed in sample-data theory. Physically, this means that it provides arbitrarily large amplification for certain inputs (e.g. noise). Non-impulsive sampling, as obtained with pre-filters, bounds this amplification.

The second task of the redirected research made use of the hybrid operator model to answer the following very basic approximation question: How well can digitally-implemented control laws mimic analog ones? More specifically, if samplers, holds and digital algorithms are all selected to best approximate a given linear, time-invariant analog system, how good can the approximation be? The answer to this question is elegantly simple: The digitally-implemented system can exactly duplicate the impulse response matrix, $G(t-\theta)$, of the analog system at all points in the t, θ-plane except on a strip of width τ (sample time) along the main diagonal $(t=\theta)$. Inside this strip, the hybrid system's impulse response must be zero on various triangular segments. Accordingly, this region of approximation has been named the "triangle strip." Details of the optimal sampling, hold,

and digital function for this approximation result are again summarized
in Section 2 and derived in detail in [6]. Its significance is that it
provides a simple and clear picture of the basic limitations inherent in
digitally-implemented controls. Such controls are fundamentally inferior
to their analog counterparts because they cannot utilize all the input
data in the triangle strip. As shown below, this limits bandwidth,
restricts performance, and precludes robustness guarantees such as those
enjoyed by the continuous-time LQ regulator.

New Research Results

Motivated by the above characterization of hybrid system limitations,
the research effort was continued to explore the qualitative and quantitative
ways in which these limitations manifest themselves in hybrid system design.
The results of this new research are reported here.

The new research examines hybrid operator models from the viewpoint
of "conic sectors theory" [Zames, 7, and Safonov, 5]. This viewpoint
encompasses the approximation results above and provide an effective way to
express their implied limitations in terms of conventional analog control
system concepts (e.g. bandwidths, loop gains, gain and phase margins, etc.).
The basic idea is to approximate hybrid operators (which may be viewed as
periodically time-varying analog systems) by time-invariant linear analog
models. These models form the "centers" of conic sectors, and their modelling

errors determine the sector "radii". The size of sector radii, in turn, determine bandwidth limitations, stability robustness reductions, and performance reductions, in accordance with existing sector-based control system design techniques [Doyle and Stein, 8, Lehtomaki, 13].

The relevant conic sector concepts and their use in analog system design are briefly developed in Section 3. They are then applied in Section 4 to hybrid operators. Two expressions are derived which define sectors radii as functions of the true hybrid operator and its time-invariant analog approximations. These expression show explicit dependences on the selected sampling rate, the selected sample- and hold filters, and the selected digital algorithm. These parameters may be chosen to minimize the radii (in an appropriate function space sense) and, thus, to minimize the bandwidth, robustness and performance limitations which the hybrid operator imposes.

The conic sector expressions from Section 4 are illustrated with a small design example in Section 5. While this example are limited in scope it serve to illustrate the use of sector-based hybrid system approximations and point the way to a general control system design philosophy which incorporates digital implementations under a more general common umbrella of feedback design for systems with approximation errors.

2. HYBRID OPERATOR MODELS

We will consider digitally-implemented control systems which can be represented by the block diagram of Figure 1. The three main functions associated with the controller block in this diagram are:

1) The **sampling operation** which converts M-dimensional analog inputs u(t) on the interval $(\ell-1)\tau \leq t \leq \ell\tau$ into N-dimensional discrete samples ξ_ℓ, $\ell = 1, 2, \ldots$,

2) the **digital algorithm** which converts the N-dimensional sequences ξ_ℓ into L-dimensional sequences η_k, $k = 0, 1, \ldots$, and

3) the **hold operation** which converts the L-dimensional sequences η_k into R-dimensional analog functions v(t) on the interval $k\tau \leq t \leq (k+1)\tau$.

The system's sample time will be designated by the symbol τ. These three functions will be assumed to have the forms

$$\xi_\ell = \int_{(\ell-1)}^{\ell\tau} f_\ell(\theta) u(\theta) d\theta = \int_{(\ell-1)\tau}^{\ell\tau} f_o(\theta - \ell\tau) u(\theta) d\theta \tag{1}$$

$$\eta_k = \sum_{\ell=1}^{k} D_{k\ell} \xi_\ell \tag{2}$$

$$v(t) = h_k(t)\eta_k = h_o(t-k\tau)\eta_k \tag{3}$$

The first of these equations is a simple analog convolution operation with weighting function (impulse response) $f_o(\lambda)$. This could be the weighting function of an analog prefilter, an approximate impulsive sample, or various other vector valued input averaging operations. Some examples are given in [6]. The second equation is a standard
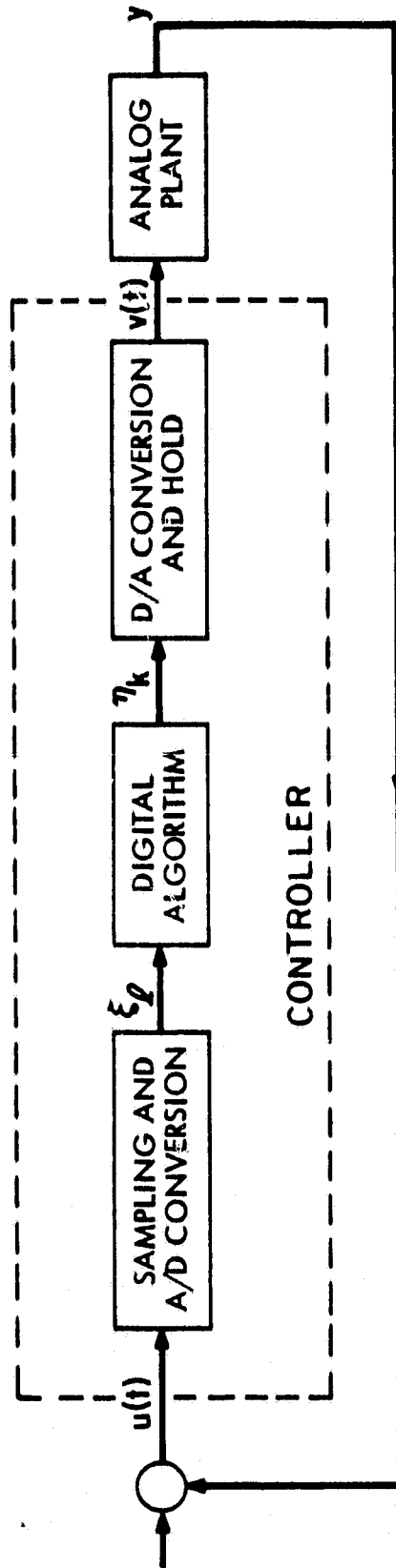
FIGURE 1: Typical Digitally-Implemented Control System.

digital convolution with coefficients $D_{k\ell}$. The third is a generalized output hold operation with weighting function $h_o(\lambda)$. This could be a simple constant to represent the common "zero-order hold," but in general it will be selected to achieve broader goals. Some examples are again given in [6]. Note that the controller is completely characterized by the two matrix-valued functions $f_o(\lambda)$, $h_o(\lambda)$ and by the coefficient matrices $D_{k\ell}$.

Hybrid Operator Representation

Given the above description of a digitally-implemented controller, it is straight-forward ([6], Section 2) to write its input-output operator representation, G, in the terms of an impulse response matrix, $G(t,\theta)$. That is,

$$\underset{\sim}{v} = G \underset{\sim}{u} \tag{4}$$

where $\underset{\sim}{v}$ and $\underset{\sim}{u}$ denote functions on $[0,\infty)$ related by the convolution

$$v(t) = \int_o^t G(t,\theta)u(\theta)d\theta \tag{5}$$

with

$$G(t,\theta) = h_o(t-k\tau) \sum_{\ell=1}^{k} D_{k\ell} f_o(\theta-\ell\tau) \tag{6}$$

Here k is understood to be the largest integer less than or equal to t/τ. We will refer to this input-output description of the controller as "the hybrid operator model" or simply as the "hybrid operator". Note that it is a time-varying linear dynamic system characterized by h_o, f_o, and $D_{k\ell}$.

Optimal Hybrid Approximation

Consider now the problem of finding a hybrid operator model $G(h_o, f_o, D_{k\ell})$ to approximate a continuous-time linear dynamic control law with impulse response matrix

$$\overline{G}(t, \theta) = Ce^{A(t-\theta)}B, \tag{7}$$

where A, B, and C are given system matrices.

Let the approximation criterion be to minimize

$$J = E\left\{ \lim_{T \to \infty} \frac{1}{T} \int_0^T ||v(t) - \overline{v}(t)||^2 dt \right\} \tag{8}$$

where $v(t)$ and $\overline{v}(t)$ are the outputs of the hybrid and pure analog controllers, respectively, when excited by the same white noise input. Then it is shown in [6], Section 4, that the optimal approximating hybrid controller has the following sampling function:

$$f_o(\lambda) = e^{-A\lambda}B \tag{9}$$

It's corresponding hold function is

$$h_o(\lambda) = Ce^{A\lambda}, \tag{10}$$

and the digital algorithm is

$$D_{k\ell} = e^{A\tau(k-\ell)}. \tag{11}$$

Moreover, these parameters cause (6) to duplicate (7) exactly everywhere except on the "triangle strip" of Figure 2. Note that the sampling
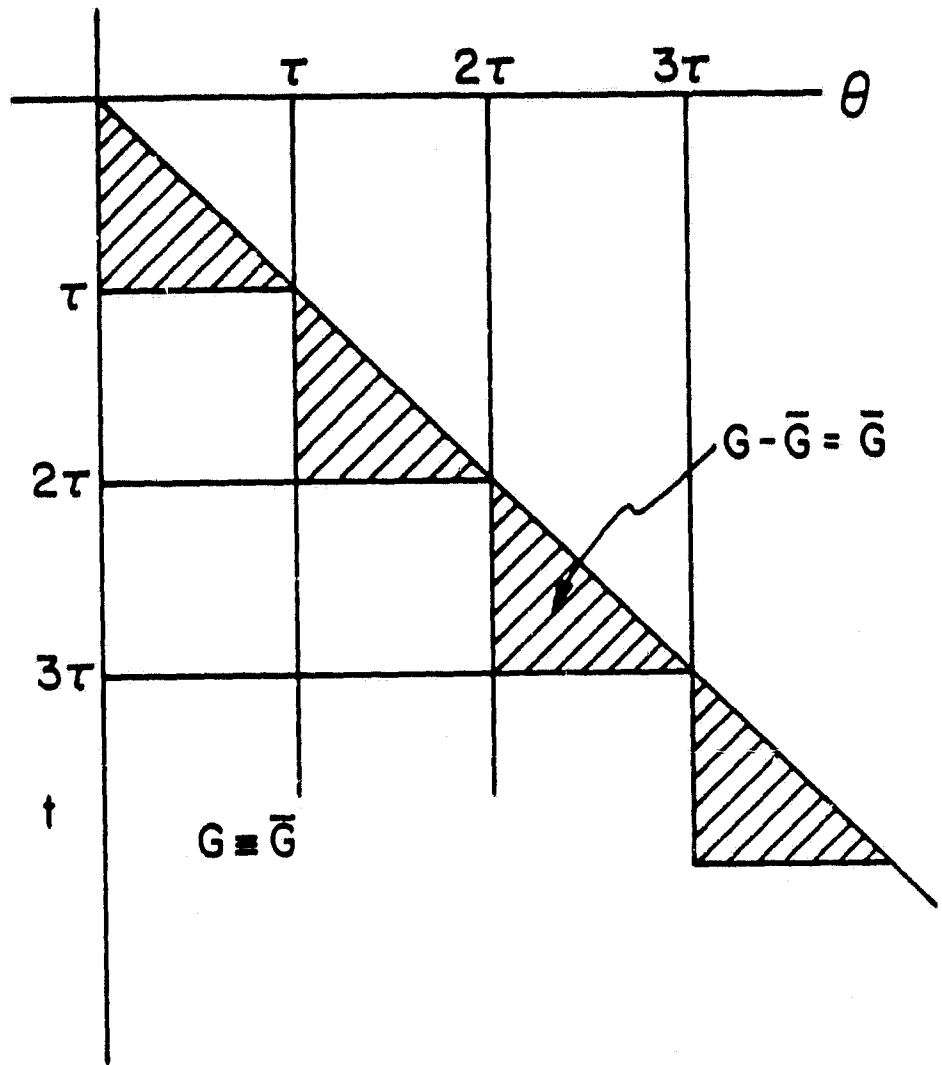
FIGURE 2:   Triangle Strip.

and hold functions (9)-(10) of this optimal hybrid approximation are themselves n-th order dynamic systems, where n is the dimension of A. Hence, the overall hybrid controller can be visualized as shown in Figure 3.

As indicated earlier, the significance of the above result is not the optimal structure in Figure 3 itself (after all, the sampling and hold functions are quite complex, each literally duplicating the analog system), but rather the fact that the inherent hybrid system limitations are so simply and clearly displayed by the triangle strip in Figure 2. It follows from this figure that the minimum approximation error is given by the error operator

$$\underset{\sim}{e} = (G - \overline{G}) \underset{\sim}{u} \tag{12}$$

where $G - \overline{G}$ has the impulse response representation

$$e(t) = \int_{k\tau}^{t} \overline{G}(t-\theta) u(\theta) d\theta \tag{13}$$

Qualitatively therefore, the hybrid system suffers an inherent time varying "data lapse" with a maximum duration of τ seconds (average $\tau/2$), and with data weighting proportional to the desired impulse response, $\overline{G}$. Hence, both the nominal function $\overline{G}$ and the sample time τ contribute to the significance of the error. Small errors are assured if $\overline{G}(\lambda)$ is small over the whole interval $0 \leq \tau \leq \tau$ and $u(\theta)$ is relatively "smooth." These observations are given further interpretation below.
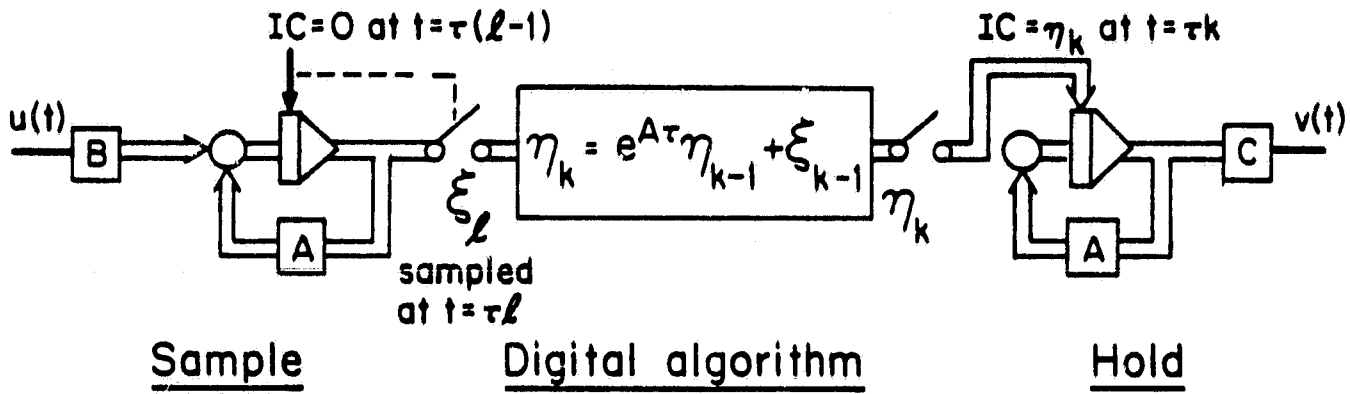
Sample   **Digital algorithm**   **Hold**

FIGURE 3: The Optimal Hybrid Compensator.

3. CONIC SECTOR CONCEPTS

The key feature of the hybrid operator model $\hat{G}$ is that it represents an analog input-output view of digitally-implemented controllers. That is, the operator maps continuous-time input functions, $\underset{\sim}{u}$ (i.e. $u(t)$, $0 \leq t < \infty$) into continuous-time output functions, $\underset{\sim}{v}$ (i.e. $v(t)$, $0 \leq t < \infty$). All inter-sample behavior such as limit cycling and aliasing is thus included in the representation. The input-output viewpoint also makes it possible to utilize certain function space notions of approximation -- in particular, the concept of conic sectors.

Conic Sectors [5,7]

In order to discuss conic sectors, it is necessary to review a number of basic concepts from functional analysis. The first of these is the function space, L_2^n. This is the collection of all n-dimensional vector-valued functions which are square integrable on $[0,\infty)$. If the function $\underset{\sim}{x}$ belongs to L_2^n, then its norm is defined by

$$||\underset{\sim}{x}|| \triangleq \left[\int_0^\infty x^T(t)x(t)dt \right]^{1/2} < \infty . \tag{14}$$

Moreover, the inner product for any two functions $\underset{\sim}{x_1}$, $\underset{\sim}{x_2}$ in L_2^n can be defined by

$$<\underset{\sim}{x_1},\underset{\sim}{x_2}> \triangleq \int_0^\infty x_1^T(t)x_2(t)dt, \tag{15}$$

It follows that

$$||\underset{\sim}{x}|| \equiv [<\underset{\sim}{x},\underset{\sim}{x}>]^{1/2} . \tag{16}$$

The chief limitation of the space L_2^n for control system analysis is that it contains no unstable functions (i.e. functions with $||\underset{\sim}{x}||=\infty$). This can be remedied by introducing the so-called extended space, L_{2e}^n. This space is the collection of all functions which are square integrable on all finite time intervals, i.e. it contains all functions x which satisfy

$$||\underset{\sim}{x}||_T \triangleq \left[\int_0^T x^T(t)x(t)dt\right]^{1/2} < \infty \quad \text{for all T} \quad . \tag{17}$$

Functions such as $x(t)=e^t$ are included in L_{2e}^1, for example, while functions such as $x(t) = \tan t$ are not.

An operator such as G is a mapping which associates each functions in its domain (the set of input functions) with exactly one function in its range (the set of output functions). For our purposes, the domain of G will be the space L_{2e}^m and its range will be some subset of L_{2e}^r. We will also assume that G is causal and L_{2e}-stable. Causality means that the output of G at time $t=t_1$ does not depend on future inputs, $t>t_1$. L_{2e}-stability means that the norms of the input and output functions of G are related as follows:

$$||G\underset{\sim}{u}||_T \leq k \, ||\underset{\sim}{u}||_T \tag{18}$$

for some $k<\infty$, all $\underset{\sim}{u}$ in L_{2e}^m, and all $T<\infty$

This implies that all bounded input functions produce bounded output functions. Note that the two norms on the right and left of this expression are different because they are defined on different

function spaces (L_{2e}^m and L_{2e}^r). Their ratio is often used to define yet
another norm for the operator itself, namely

$$\|G\| \triangleq \sup_{\|\underset{\sim}{u}\|_T \neq 0} \frac{\|G\underset{\sim}{u}\|_T}{\|\underset{\sim}{u}\|_T} \tag{19}$$

This is the so-called induced operator norm, induced by norms on L_{2e}^m
and L_{2e}^r. It is a common abuse of notation in the functional analysis
literature to use the same symbols, $\|\cdot\|$, for function norms and for
induced operator norms. The distinction is made clear by the arguments
used with the symbol.

Given these preliminaries, the operator G can be viewed as a subset
of the crossproduct space $L_{2e}^m \times L_{2e}^r$. This is shown schematically in
Figure 4, where input functions are represented by points along the x-axis,
and the operator is represented by the graph itself. Within this pictorial
framework, a conic sector is a cone-shaped subset of $L_{2e}^m \times L_{2e}^r$ which
contains many potential operator graphs. In mathematical terms, it is the
collection of all operators, H, which satisfy

$$\langle H\underset{\sim}{u}-(C+R)\underset{\sim}{u},\ H\underset{\sim}{u}-(C-R)\underset{\sim}{u}\rangle_T \leq 0\ ,\quad \text{for all }\ T<\infty\ \text{ and all }\ \underset{\sim}{u}\in L_{2e}^m \tag{20}$$

Here $\langle\cdot,\cdot\rangle_T$ is the inner product on L_{2e}^r and C and R are causal,
L_{2e}-stable operators. C and R define the boundaries of the conic sector
and are called the "cone center" and "cone radius", respectively, for obvious
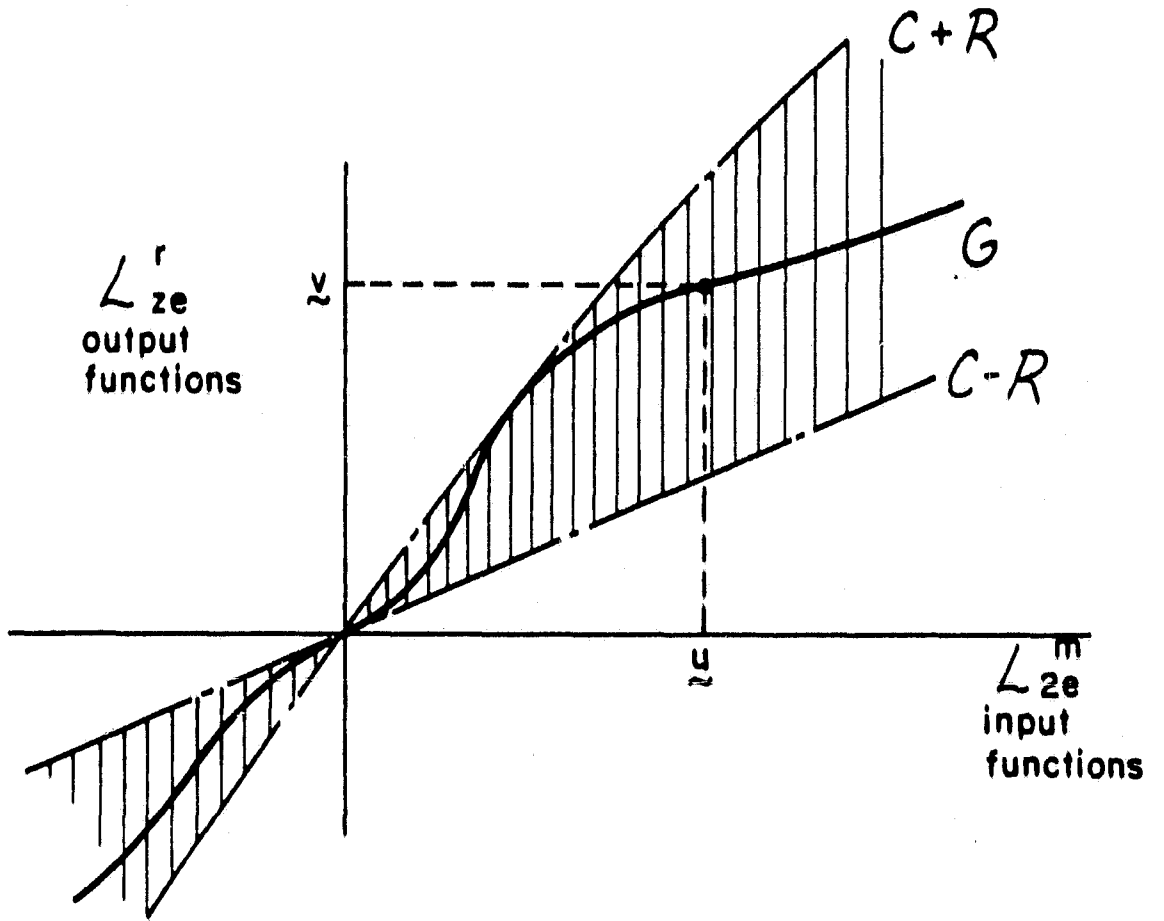geometric reasons.

FIGURE 4: Conic Sector (C,R)

Using elementary manipulations of (20), it is possible to show that conic sectors provide a way to approximate G by C. This is done as follows: Suppose (20) is satisfied by $H=G$ [i.e. G is a member of Sector (C,R)]. Then

$$\langle G\underset{\sim}{u} - (C+R)\underset{\sim}{u}, \ G\underset{\sim}{u} - (C-R)\underset{\sim}{u}\rangle_T$$

$$= \langle(G-C)\underset{\sim}{u} - R\underset{\sim}{u}, \ (G-C)\underset{\sim}{u} + R\underset{\sim}{u}\rangle_T$$

$$= \langle(G-C)\underset{\sim}{u}, \ (G-E)\underset{\sim}{u}\rangle_T - \langle R\underset{\sim}{u}, R\underset{\sim}{u}\rangle_T \leq 0$$

$$\text{for all } T<\infty \text{ and all } \underset{\sim}{u} \in L_{2e}^m \quad (21)$$

Hence,

$$||(G-C)\underset{\sim}{u}||_T \leq ||R\underset{\sim}{u}||_T \quad (22)$$

$$\text{for all } T<\infty \text{ and all } \underset{\sim}{u} \in L_{2e}^m$$

This shows that the output of C approximates the output of G within approximation error bounded by the norm of the radius operator R. Note from (22) that sector membership also implies that

$$||(G-C)\mathcal{D}|| \leq ||R\mathcal{D}|| \quad (23)$$

for any operator $\mathcal{D}$.

Sector-Based Feedback Design

In the last several years, the conic sector concept has been recognized as an important tool in feedback analysis and design [Safonov,5, Zames,7, Doyle and Stein,8, Lehtomaki,13]. The basic idea is that very complicated plant operators G (perhaps nonlinear, infinite

dimensional, time-varying, etc.) can be reliably approximated by simple cone centers C (usually linear time-invariant finite dimensional systems), provided that the approximation error is properly accounted for in the design process. This "proper accounting" usually means that a design based on C must be restricted to maintain stability robustness, and its performance goals must be relaxed to account for inherent degradations. These restrictions generally increase as the magnitudes of approximation errors grow. The basic relationships between design restrictions and conic sector approximation errors are summarized below.

Stability Robustness Restrictions -- We will treat the generic feedback problem where G is the loop transfer operators of a unity feedback loop, as shown in Figure 5. G is assumed to be any causal, L_{2e}-stable member of Conic Sector (C, R) for which the feedback loop is "well-posed" [Willems, 9]. This means that $(I+G)^{-1}$ exists and is causal. We will also assume that the nominal feedback operator $(I+C)^{-1}$ is L_{2e}-stable. Then the loop's errors in response to disturbances, $\underset{\sim}{d}$, and reference commands, $\underset{\sim}{c}$, are given by

$$
\begin{aligned}
\underset{\sim}{e} &\overset{\Delta}{=} \underset{\sim}{c} - \underset{\sim}{y} \\
&= (I+G)^{-1}(\underset{\sim}{c}-\underset{\sim}{d}) \\
&= [I+C+(G-C)]^{-1}(\underset{\sim}{c}-\underset{\sim}{d}) \\
&= (I+C)^{-1}[I+(G-C)(I+C)^{-1}]^{-1}(\underset{\sim}{c}-\underset{\sim}{d})
\end{aligned}
\tag{24}
$$
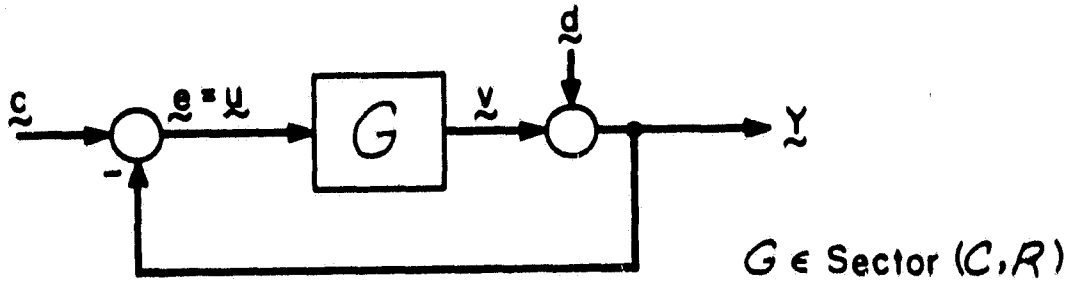
FIGURE 5: Generic Feedback Loop.

All inverses in this expression exist and are causal by assumption. Moreover, $(I+C)^{-1}$ is stable by assumption. It then follows that e will be bounded and the feedback loop will be stable in the sense of (18) if and only if the operator

$$[I+(G-C)(I+C)^{-1}]^{-1}$$

is stable. As shown in [Sandell, 10], this stability requirement is assured whenever

$$||(G-C)(I+C)^{-1}|| < 1 \tag{25}$$

or, using (23), whenever

$$||R(I+C)^{-1}|| < 1 \tag{26}$$

or equivalently, whenever

$$||RC^{-1}[C(I+C)^{-1}]|| < 1 \tag{27}$$

and C^{-1} exists.

Equation (27) shows that stability can be achieved for all plants in the Conic Sector (C,R) if the feedback system's nominal closed loop responses, $C(I+C)^{-1}$, are restricted to be small for all inputs which have large normalized conic sector approximation errors, RC^{-1}. A frequency domain interpretation of this restriction is given shortly.

<u>Performance Degradation</u> -- Looking beyond mere stability, equation (24) can also be used to show that sector approximation errors impose inherent degradations in the performance of feedback systems. In accordance with

our input-output viewpoint, we will evaluate performance in terms of
the error magnitudes generated for some specified subset of disturbance
and/or command functions. That is, let $S \subset L_{2e}^r$ be a specified set of
functions (say, all sinewaves with frequency less than ω_0) and let $q \geq 0$
be the smallest scalar such that

$$||\underset{\sim}{e}||_T = ||(I+G)^{-1}(\underset{\sim}{c}-\underset{\sim}{d})||_T \leq q||\underset{\sim}{c}-\underset{\sim}{d}||_T \tag{28}$$
$$\text{for all } (\underset{\sim}{c}-\underset{\sim}{d}) \in S \text{ and all } T < \infty$$

Then q will be taken as a quality measure for the feedback system's
performance.

We will assume that the nominal system has quality measure $q = q_0$,
with q_0 designed to be sufficiently small. The question then is to
determine the actual value of q which applies in the presence of sector
approximation errors. While it is generally difficult to compute this
value exactly, equation (24) can be readily manipulated to obtain a
useful upper bound. In particular, from (24)

$$\underset{\sim}{e} = (I+C)^{-1}(\underset{\sim}{c}-\underset{\sim}{d}) + (I+C)^{-1}\underset{\sim}{\Delta c} \tag{29}$$

with

$$\underset{\sim}{\Delta c} = \{[I+(G-C)(I+C)^{-1}]^{-1}-I\}(\underset{\sim}{c}-\underset{\sim}{d})$$
$$= -\{[I+(G-C)(I+C)^{-1}]^{-1}(G-C)(I+C)^{-1}\}(\underset{\sim}{c}-\underset{\sim}{d}) \tag{30}$$

Since we have already established conditions for the inverse in the last
expression to be stable, it follows that under those same conditions

$$||\underset{\sim}{\Delta c}||_T \leq \frac{1}{1-||R(I+C)^{-1}||} ||R(I+C)^{-1}(\underset{\sim}{c}-\underset{\sim}{d})||_T \tag{31}$$

and using (31) in (29) we have

$$\left|\left|\underset{\sim}{e}\right|\right|_T \leq \left|\left|(I+C)^{-1}(\underset{\sim}{c}-\underset{\sim}{d})\right|\right|_T + \frac{\left|\left|(I+C)^{-1}\right|\right|}{1-\left|\left|R(I+C)^{-1}\right|\right|} \left|\left|R(I+C)^{-1}(\underset{\sim}{c}-\underset{\sim}{d})\right|\right|_T \quad . \quad (32)$$

This equation requires careful interpretation. Note that the first term
on the right hand side is simply the performance of the nominal system.
Hence, for inputs restricted to the specified set, $(\underset{\sim}{c}-\underset{\sim}{d}) \in S$, we have

$$\left|\left|(I+C)^{-1}(\underset{\sim}{c}-\underset{\sim}{d})\right|\right|_T \leq q_o \left|\left|\underset{\sim}{c}-\underset{\sim}{d}\right|\right|_T \quad . \quad\quad (33)$$

The second term on the right hand side has three elements:

   Element (1): $\left|\left|(I+C)^{-1}\right|\right|$
   This is the (global) norm of the nominal
   sensitivity operator and will be denoted by s*
   Note that s* can never be less than unity with
   strictly proper plants since for these there
   exist functions d such that $C\underset{\sim}{d}$ is arbitrarily
   small. In well designed systems, however, s*
   approaches unity quite closely.

   Element (2): $1-\left|\left|R(I+C)^{-1}\right|\right|$
   This is a (global) stability margin of the feedback
   system and will be denoted by m*. From (26), its value
   is guaranteed to be positive if the system is stable.
   Typical values for well designed systems hover around
   0.5.

   Element (3): $\left|\left|R(I+C)^{-1}(\underset{\sim}{c}-\underset{\sim}{d})\right|\right|_T$
   This is the function norm of the sector radius operator,
   operating on the nominal feedback errors. For inputs

restricted to S, let the radius operator satisfy

$$||R\underset{\sim}{e}||_T \leq r_0 ||\underset{\sim}{e}||_T \tag{34}$$

for all $\underset{\sim}{e} \in (I+C)^{-1} S$ and all $T < \infty$. Then

$$||R(I+C)^{-1}(\underset{\sim}{c}-\underset{\sim}{d})||_T \leq r_0 q_0 ||\underset{\sim}{c}-\underset{\sim}{d}||_T \tag{35}$$

with $r_0 q_0$ necessarily less than unity from (26)

Putting these elements together allows us to reduce (32) to the following simple form:

$$||\underset{\sim}{e}||_T \leq (1+ \frac{s^*}{m^*} r_0)q_0 ||\underset{\sim}{c}-\underset{\sim}{d}||_T \tag{36}$$

for all $(\underset{\sim}{c}-\underset{\sim}{d}) \in S$ and all $T < \infty$

This show that sector approximation errors degrade feedback performance in a direct and simple way. The nominal quality measure is simply scaled upward by the factor $1+s^* r_0/m^*$. The latter increases with increasing sector approximation errors on the function set S, and also with deteriorating global sensitivity and stability margin properties of the nominal design.

Frequency Domain Interpretations -- If the cone parameters C and R are stable linear, time-invariant operators, then the norm inequalities in (26),(27) and (36) can be readily evaluated with classical frequency-domain methods. This is done with the following norm identity for linear time invariant operators [Desoer and Vidyasagar, 11]

$$||C|| = \max_\omega \bar{\sigma}[C(s)]|_{s=j\omega} \tag{37}$$

where $C(s)$ is the (matrix-valued) Laplace transform of the impulse response, $C(t)$, of the operator C, and $\bar{\sigma}[\cdot]$, $\underline{\sigma}[\cdot]$ denote its maximum and minimum singular values[†]. Using (37), it follows that (26) and (27) are satisfied if

$$\bar{\sigma}[R(j\omega)] \leq \underline{\sigma}[I+C(j\omega)] \qquad \text{for all } 0 \leq \omega < \infty \tag{26'}$$

or

$$\bar{\sigma}[RC^{-1}(j\omega)] \leq \sigma[C(j\omega)(I+C(j\omega))^{-1}] \tag{27'}$$
$$= \underline{\sigma}[I+C^{-1}(j\omega)] \qquad \text{for all } 0 \leq \omega < \infty$$

Note that (27)' imposes explicit magnitude constraints on the nominal frequency response. At all frequencies where the normalized error, $RC^{-1}(j\omega)$, is large (compared with unity), the inverse loop transfer matrix $C^{-1}(j\omega)$ must also be large, and hence, the loop transfer matrix itself must be small. Since $RC^{-1}(j\omega)$ typically grows at higher frequencies, this constraint imposes explicit limitations on achievable crossover frequencies and on closed loop bandwidths.

Note that conic sector approximation errors play identical roles in the above sense to any other modelling errors already recognized in the design process.

The performance degradation equation (36) can be similarly interpreted. We get

---

[†] We will use the same symbol (C) to denote both the impulse response and its transfer functions. The differentiation will be made clear by arguments.

$$s^* = \max_{0 \le \omega < \infty} \bar{\sigma}[(I+C(j\omega))^{-1}]$$

$$\equiv \min_{0 \le \omega < \infty} \frac{1}{\underline{\sigma}[I+C(j\omega)]} \tag{38}$$

$$m^* = 1 - \max_{\omega} \bar{\sigma}[RC^{-1}(j\omega)]/\underline{\sigma}[I+C^{-1}(j\omega)] \tag{39}$$

and letting S be the set of all sine waves with frequency less than ω_0,

$$q_0 = \min_{0 \le \omega < \omega_0} \frac{1}{\underline{\sigma}[I+C(j\omega)]} \tag{40}$$

$$r_0 = \min_{0 \le \omega < \omega_0} \bar{\sigma}[R(j\omega)] . \tag{41}$$

When substituted into (36), these equations show that performance degradation due to sector approximation errors can be minimized by designing good nominal sensitivity and stability margin properties over the entire frequency range (small s^*, large m^*) and by assuming small sector approximation errors over $\omega \le \omega_0$ (small r_0).

4. CONIC SECTORS FOR THE HYBRID OPERATOR

Motivated by the above discussion of conic sector concepts in feedback design, this section proceeds to derive two expressions for radii of conic sector approximations of the hybrid operator developed in Section 2. The first expression is based on time-domain analysis and yields a conservative non-dynamic radius. The second expression is based on frequency-domain analysis and yields a sharper dynamic radius operator. Some examples using the second radius are given in Section 5.

A Non-Dynamic Radius

We found in Section 2 that the hybrid operator is a linear, time-varuing convolution operator with impulse response matrix $G(t,\theta)$ defined by equation (6). Our objective now is to approximate this operator by a linear time-invariant convolution with impulse response $C(t-\theta)$. The approximation error should be such that it can be bounded by a sector radius operator as in equation (22).

To achieve the latter objective, consider the convolution operator for the error, i.e.

$$\underset{\sim}{e} \overset{\Delta}{=} (G-C)\underset{\sim}{u}$$

with

$$e(t) = \int_0^t [G(t,\theta)-C(t-\theta)]u(\theta)d\theta$$

$$= \int_0^t \Delta G(t,\theta)u(\theta)d\theta , \qquad t\geq 0 \qquad (42)$$

This expression can be bounded as follows:

$$||G-C||^2 = \sup_{T,\,||\underset{\sim}{u}||_T=1} \left[\int_0^T e^T(t)e(t)dt \right]$$

$$= \sup_{..} \left[\int_0^T dt \int_0^t d\theta \int_0^t d\lambda \; u^T(\theta)\Delta G^T(t,\theta)\Delta G(t,\lambda)u(\lambda) \right]$$

$$\leq \sup_{..} \left[\int_0^T dt \int_0^t d\theta \int_0^t d\lambda \; |u^T(\theta)|\bar{\sigma}[\Delta G(t,\theta)]\bar{\sigma}[\Delta G(t,\lambda)]|u(\lambda)| \right] \tag{43}$$

Now let $m(t)$ be a scalar-valued function such that

$$\bar{\sigma}[\Delta G(t,\theta)] \leq m(t-\theta) \qquad\qquad \forall t,\theta \tag{44}$$

The right hand side of (43) is then bounded by

$$\sup_{T,\,||\underset{\sim}{\omega}||_T=1} \left[\int_0^t dt \int_0^t d\theta \int_0^t d\lambda \; \omega(\theta)m(t-\theta)m(t-\lambda)\omega(\lambda) \right]$$

$$= ||M||^2 \tag{45}$$

Here M is a scalar convolution operator defined by

$$\underset{\sim}{v} = M\underset{\sim}{\omega}$$

with

$$v(t) = \int_0^t m(t-\theta)\omega(\theta)d\theta \,, \qquad t\geq 0 \,. \tag{46}$$

Using (37), it now follows that a bound on the error operator (42) can

be expressed in terms of the Laplace transform, m(s), cf (46). That is,

$$\left|\left|G-C\right|\right| \leq \max_{\omega} m(s) \Big|_{s=j\omega} \overset{\Delta}{=} r \tag{47}$$

Moreover, since $m(t) \geq 0$ for all t, it can be shown that the maximum

in (47) occurs at $\omega=0$ and hence

$$r = m(s) \Big|_{s=0} = \int_0^\infty m(t)\,d\theta \tag{48}$$

In light of (47), the operator

$$\underset{\sim}{v} = R\underset{\sim}{u}$$

defined by

$$v(t) = ru(t), \qquad t \geq 0 \tag{49}$$

forms a valid radius for the sector approximation.

Note however, that the calculation of this radius if formidable.
It requires the following steps:

1)   Impulse response evaluation

$$\Delta G(t,\theta) = G(t,\theta) - c(t-\theta)$$

2)   Singular values calculations

$$\overline{\sigma}[\Delta G(t,\theta)] \qquad \forall t,\theta$$

3) Function maximization

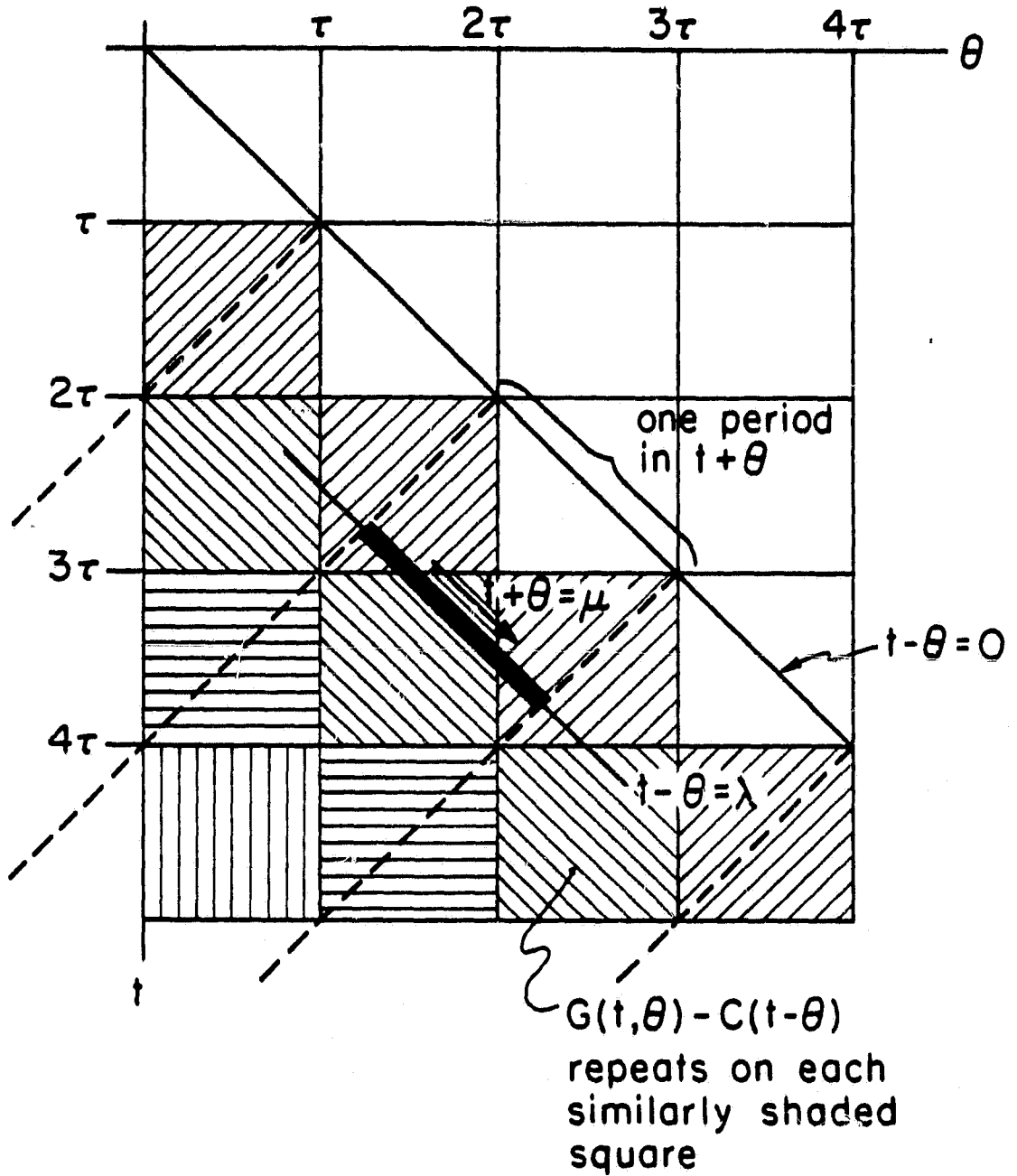$$\bar{\sigma}[\Delta G(t,\theta)] \leq m(t-\theta) \qquad \forall t,\theta$$

4) Integration

$$r = \int_0^\infty m(t)dt$$

The most difficult of these steps is 3) which requires that we find an integrable bounding function for $\bar{\sigma}[\Delta G]$ over the entire t,θ-plane. This step is made substantially easier by noting that the error operator is periodic along the $(t+\theta)$-axis whenever the digital convolution coefficients $D_{k\ell}$ in equation (6) satisfy $D_{k\ell} = D_{k-\ell} \quad \forall k,\ell$. We then need to maximize only over a single period for each value of the time index $t-\theta$, as illustrated in Figure 6.

A Dynamic Radius

In addition to its computational difficulties, the radius operator (49) suffers from conservatism. Note that its impulse response is a delta function, and hence, its Laplace transform is constant. It therefore assigns the same conic sectors error levels to low frequency inputs as it does to high frequency ones. This is inconsistent with experience. We know that a digital controller can approximate signals at $\omega \ll \frac{\pi}{\tau}$ with much greater fidelity than it can approximate signals at $\omega \geq \frac{\pi}{\tau}$. This emperical fact is not captured by (49).

ORIGINAL PAGE IS
OF POOR QUALITY

one period
in $t+\theta$

$t+\theta=\mu$

$t-\theta=0$

$t-\theta=\lambda$

$G(t,\theta)-C(t-\theta)$
repeats on each
similarly shaded
square

$$m(\lambda) = \max_{0 \le \mu \le \lambda} \Delta G(t,\theta) \bigg|_{\substack{t=(\mu+\lambda)/2 \\ \theta=(\mu-\lambda)/2}}$$

FIGURE 6:   Calculation of m(t).

An alternate radius which captures this frequency dependance has been developed by means of the following classical arguments. We start with the fact that the hybrid operator can be represented in the classical sample data, block diagram form shown in Figure 7. [Franklin and Powell, 12].
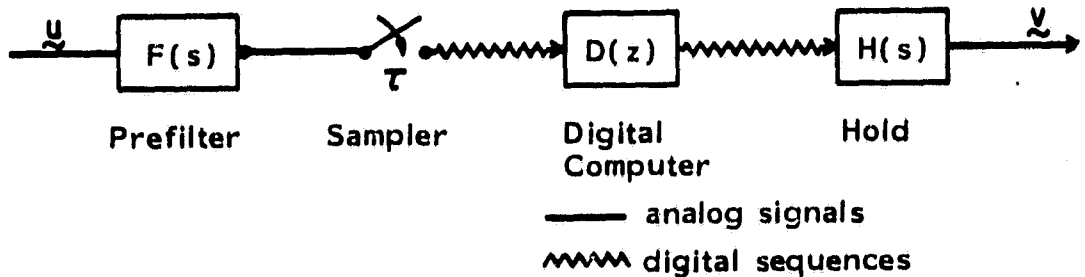
FIGURE 7: The Hybrid Compensator's Sample Data Block Diagram.

While we cannot find a Laplace or Fourier transform for this operator, it is possible to find the transforms of the output functions produced by particular inputs. Namely

$$v(j\omega) = \frac{1}{\tau} H(j\omega) D(e^{j\omega\tau}) \left[\sum_{k=-\infty}^{\infty} F(j\omega - j\omega_s k) u(j\omega - j\omega_s k) \right] \qquad (50)$$

where $D(e^{j\omega\tau})$ is the z-transform of the digital convolution sequence evaluated at $z = e^{j\omega\tau}$, and where the infinite sum with $\omega_s = \frac{2\omega}{\tau}$ represents the effect of sampling. The analog signal before the sampler has the

Fourier transform $F(j\omega)u(j\omega)$. After the sampler, the signal is mathematically represented by a sequence of impulses whose transform is the infinite sum. For notational convenience, we will represent this sum simply by $(\sum_k F_k u_k)$, where F_k and u_k are $F(j\omega-j\omega_s k)$ and $u(j\omega-j\omega_s k)$, respectively.

Using (50) in Parseval's theorem and assuming that all functions are in L_2^1, we can now write expressions for the hybrid operator's errors:

$$||(G-C)\underset{\sim}{u}||^2 = \frac{1}{2\pi}\int_{-\infty}^{\infty}\left|v(j\omega) - C(j\omega)u(j\omega)\right|^2 d\omega$$

$$= \frac{1}{2\pi}\int_{-\infty}^{\infty}\left|\frac{1}{\tau}HD(\sum_k F_k u_k) - Cu\right|^2 d\omega$$

$$= \frac{1}{2\pi}\int_{-\infty}^{\infty}\left|\sum_k G_k u_k\right|^2 d\omega \tag{51}$$

with

$$G_k = \begin{cases} \frac{1}{\tau}HDF_k & k\neq 0 \\ \frac{1}{\tau}HDF_0 - C & k=0 \end{cases} \tag{52}$$

Using Schwartz's inequality, (51) can be bounded from above.

$$||(G-C)\underset{\sim}{u}||^2 \leq \frac{1}{2\pi}\int_{-\infty}^{\infty}\left(\sum_k|G_k|^2\right)\left(\sum_\ell |u_k|^2\right)d\omega . \tag{53}$$

Now adding and subtracting $\left|\frac{1}{\tau} HDF_0\right|$ in the first sum of (53) and interchanging the order of integration and summation converts the bound to

$$\frac{1}{2\pi} \sum_{\ell} \int_{-\infty}^{\infty} \left\{ \frac{1}{\tau 2} |H|^2 |D|^2 \left(\sum_k |F_k|^2 \right) + \left| \frac{1}{\tau} HDF_0 - C \right|^2 - \left| \frac{1}{\tau} HDF_0 \right|^2 \right\} |u_\ell|^2 d\omega \qquad (54)$$

In each of these integrals we now perform a change of variables, $\omega = \omega' + \omega_s \ell$. Note that this is a frequency shift by integral numbers of sample frequencies, ω_s. Hence, the periodic functions $|D|^2$ and $\left(\sum_k |F_k|^2 \right)$ remain unchanged. We also re-interchange the order of summation and integration. This gives

$$||(G-C)\underset{\sim}{u}||^2 \le \frac{1}{2\pi} \int_{-\infty}^{\infty} \left(\sum_{\ell} \left| \frac{1}{\tau} H_\ell \right|^2 \right) |D|^2 \left(\sum_k |F_k|^2 \right) |u|^2 d\omega'$$

$$+ \frac{1}{2\pi} \int_{-\infty}^{\infty} \left(\sum_{\ell} \left| \frac{1}{\tau} H_\ell DF_\ell - C_\ell \right|^2 \right) |u|^2 d\omega'$$

$$- \frac{1}{2\pi} \int_{-\infty}^{\infty} \left(\sum_{\ell} \left| \frac{1}{\tau} H_\ell \right|^2 |D|^2 |F_\ell|^2 \right) |u|^2 d\omega' \qquad (55)$$

Note that the right hand side of (55) has the form $\frac{1}{2\pi} \int |R|^2 |u|^2 d\omega$, which according to Parseval's theorem, is equal to the norm $||R\underset{\sim}{u}||^2$.

Comparing this to our sector definition in equation (22) (restricted to L_2^1 functions) then shows that (55) represents a valid sector radius for our hybrid operator. The center of this sectors can be arbitrary. However, it is evident from (55) that the choice C^* with Fourier transform

$$C^*(j\omega) = \frac{1}{\tau} H(j\omega) D(j\omega) F(j\omega) \tag{56}$$

generates the smallest radius, R^*, with Fourier transform

$$|R^*(j\omega)|^2 = (\sum_{\ell} |\frac{1}{\tau} H_\ell|^2) |D|^2 (\sum_{k} |F_k|^2) - \sum_{\ell} |\frac{1}{\tau} H_\ell|^2 |D|^2 |F_\ell|^2$$

$$= \sum_{\ell} \sum_{k \neq \ell} | \frac{1}{\tau} |H(j\omega + j\omega_s \ell)|^2 |D(e^{j\omega\tau})|^2 |F(j\omega + j\omega_s k)|^2 \tag{57}$$

The sector defined by these expressions is explored by a simple example in the next section.

5. AN EXAMPLE

The second sector developed in Section 4 is illustrated here with a classical lead-lag compensator example. While this is a very simple example, it captures the essential issues of sector-based approximations and serves to illustrate their potential utility.

The Analog System

We start with the analog compensator

$$G_a(s) = \frac{10(s+.1)}{s+1} \tag{58}$$

We show how to implement this compensator using a digital computer, and then how to compute the center and radius of its Sector (C, R).

The digital computer is embedded in the hybrid compensator as in Figure 7. We arbitrarily choose a sample interval of $\tau = .6283$ seconds, which places the sampling frequency at $2\pi/\tau = 10$ radians per second, which is ten times the frequency of the pole location. The z-transform D(z) (used for the digital computer) is computed by the classical pole-zero mapping technique [12]. The pole at s=-1 maps to a pole at $z = e^{s\tau} = .5335$, and the zero at s=-.1 maps to a zero and $z = e^{s\tau} = .9391$. The constant is chosen so that D(z) at z=1 is equal to $G_a(s)$ at s=0. The result is

$$D(z) = 7.660 \ \frac{z-.9391}{z-.5335} \tag{59}$$

The prefilter $F(s)$ is chosen to be a low pass filter with a single pole at $s=-\pi/\tau$. The result is

$$F(s) = \frac{5}{s+5} \quad . \tag{60}$$

The hold device is chosen to be a zero-order-hold, which has the Fourier transform

$$\frac{1}{\tau} H(j\omega) = \frac{1-e^{-j\omega\tau}}{j\omega\tau} \quad , \tag{61}$$

Two Cone Centers

According to equation (56), the cone center $C^*(j\omega)$ is the given by

$$C^*(j\omega) = \left[\frac{1-e^{-j\omega\tau}}{j\omega\tau}\right]\left[7.66\,\frac{e^{j\omega\tau}-.9391}{e^{j\omega\tau}-.5335}\right]\left[\frac{5}{j\omega+5}\right] \tag{62}$$

Note that this choice of cone center has the special property of being the "straight through path," formed by replacing the sampler in Figure 7 with the gain term $\frac{1}{\tau}$ as shown in Figure 8.

$$u(j\omega) \rightarrow \boxed{F(j\omega)} \rightarrow \boxed{\frac{1}{\tau}} \rightarrow \boxed{D(e^{j\omega})} \rightarrow \boxed{H(j\omega)} \rightarrow v(j\omega)$$

FIGURE 8: The Straight Through Path.

Unfortunately, this choice also has the undesirable property of being infinite dimensional and difficult to work with in state space realizations. For this reason, we will also examine an alternate center which approximates (62) by a low order state space model. This alternate choice is

$$C(j\omega) = \left[\frac{2}{j\omega\tau+2}\right]\left[\frac{10(j\omega+.1)}{j\omega+1}\right]\left[\frac{5}{j\omega+5}\right] \tag{63}$$

and is obtained by approximating the zero order hold with a first order filter and replacing $D(e^{j\omega\tau})$ with $G_a(j\omega)$.

Cone Radii

Following our previous derivation, the cone radius corresponding to center $C^*(s)$ is given by equation (57). The radius for $C(s)$, on the other hand, requires a slight modification of this equation to account for difference between C and C^*. The appropriate modification is obtained from (55) and has the form

$$|R(j\omega)|^2 = \sum_{\ell}\left[\sum_{k\neq\ell}|\frac{1}{\tau}H_\ell|^2|D|^2|F_k|^2 + |C_\ell-C_\ell^*|^2\right] \tag{64}$$

Both equations (57) and (64) can be evaluated numerically by computing the infinite sums over k and ℓ. It can be shown that these sums converge for all functions H, F, and C-C* which roll off as least as fast as $1/\omega$ at high frequencies. In fact, if the roll-off is $1/\omega$ exactly, then the convergence properties of each sum are proportional to

$$\sum_{\ell=1}^{\infty}\frac{1}{\ell^2} = \frac{\pi^2}{6} = 1.644934 \tag{65}$$

We have empirically determined that these infinite sums can be
terminated at plus and minus 20 terms. Their general convergence pro-
perties, however, still need to be better understood.

Graphical Results

The net results of all these calculations are best viewed as
conventional Bode plots of the various functions involved. We start
with Figures 9a and 9b, which show gain and phase characteristics of
the zero order hold, $\frac{1}{\tau} H$, and its first order approximation. Note
that the approximation is good up to about 2.4 rps, or roughly $\omega_s/4$.

Figures 10a and b show Bode plots of the analog lead compensator,
$G_a(s)$ and the two centers, $C(s)$ and $C^*(s)$. Note that these centers have
more phase lag than the analog compensator, due to the extra lag added by
the prefilter and hold. However, C and C* again track closely up to
about 2.5 r/s.

The corresponding radii were computed according to equations (57)
and (64). One of the required infinite sums is shown in Figure 11. We
see that above $2\pi/\tau = 10$ radians the infinite sum is approximately unity.
The radii themselves are plotted in Figure 12. We see that they agree
closely for high frequencies ($\omega \geq 1$ rad/sec) but differ substantially at
lower frequencies. This difference is caused by the $\left|C^*_\ell - C_\ell\right|^2$ terms in
(64). Note that the sum of these terms alias high frequency differences
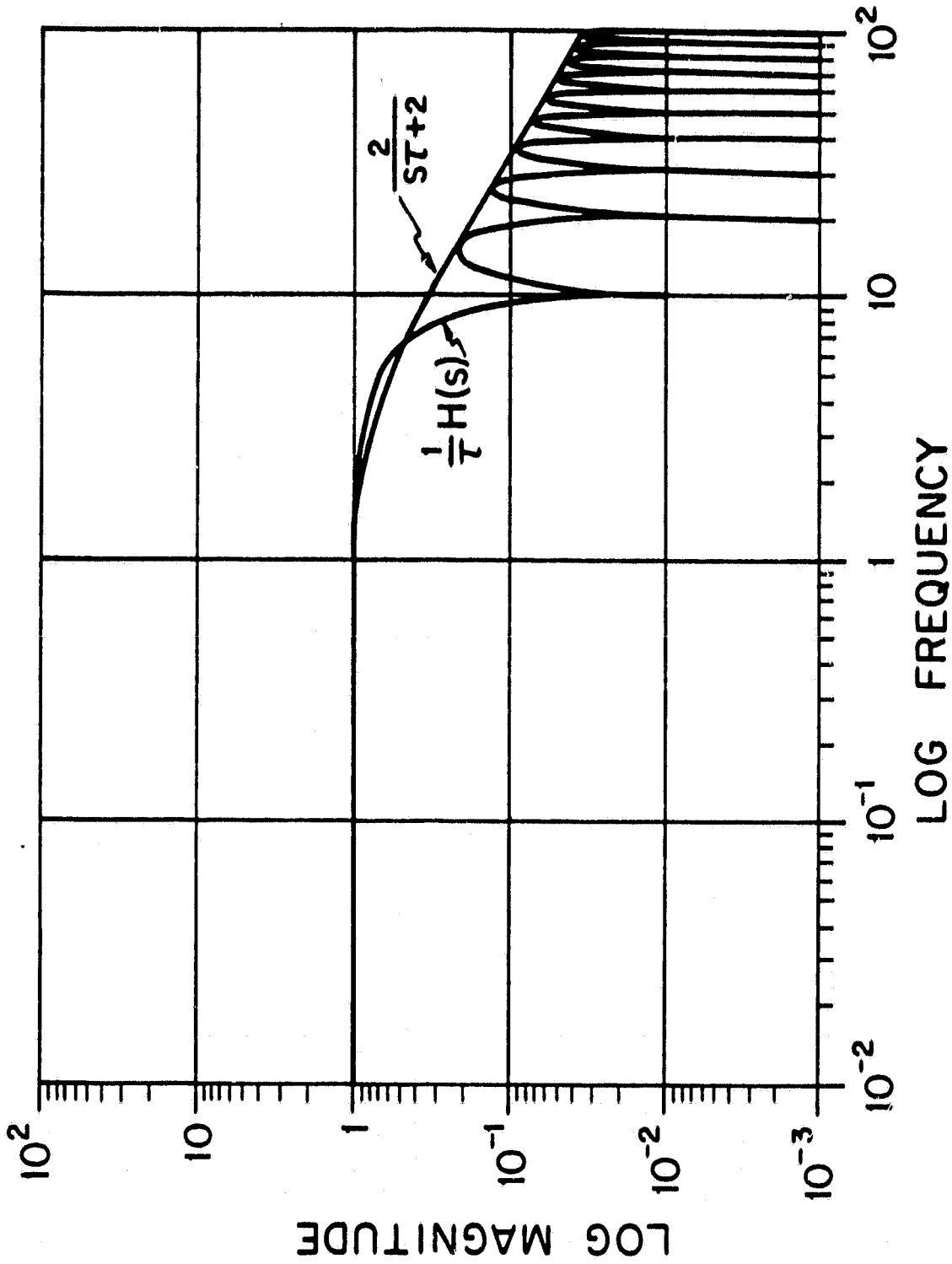between C* and C down to lower frequencies. In particular, the differences
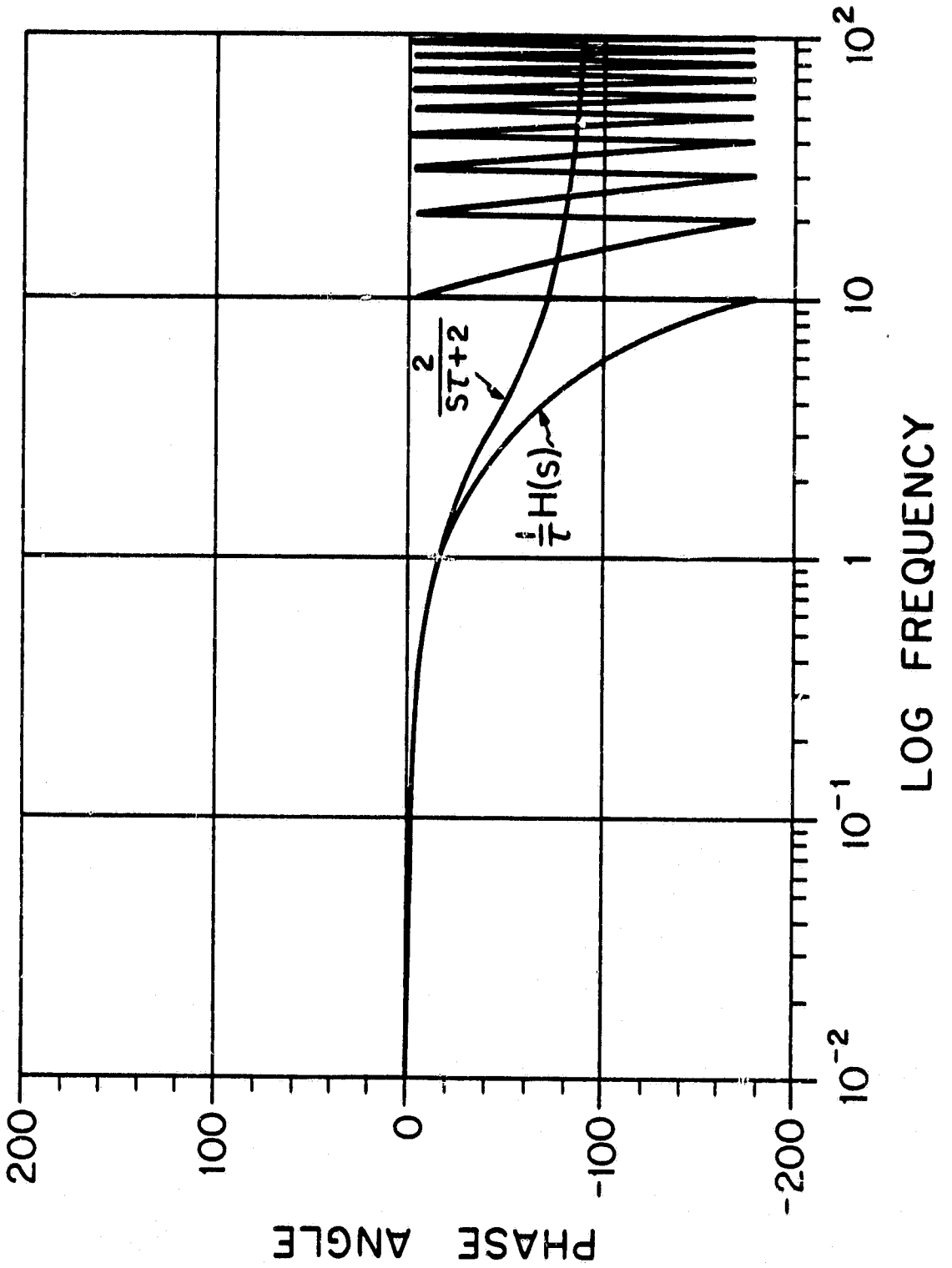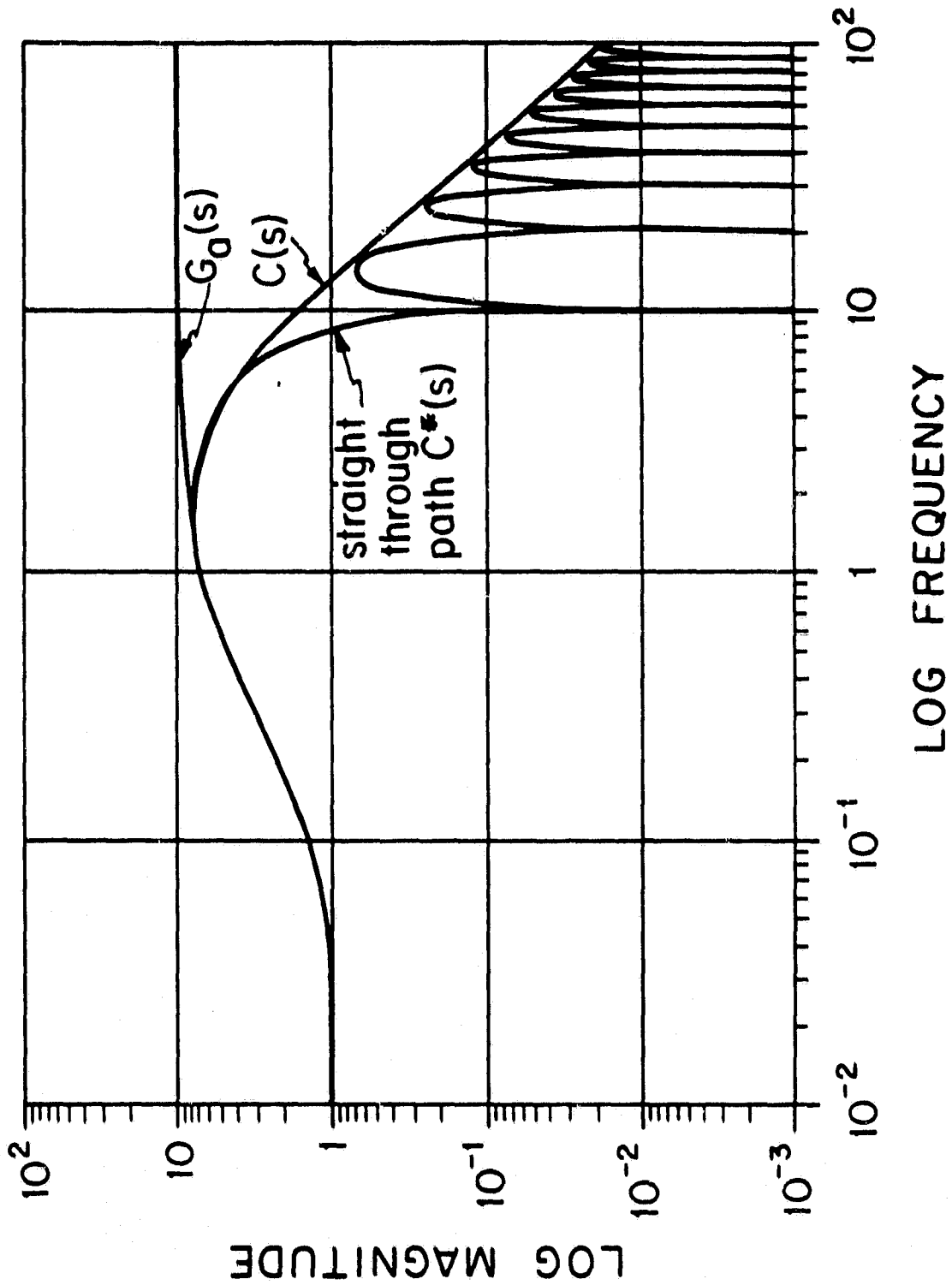
FIGURE 9a: Zero-Order-Hold

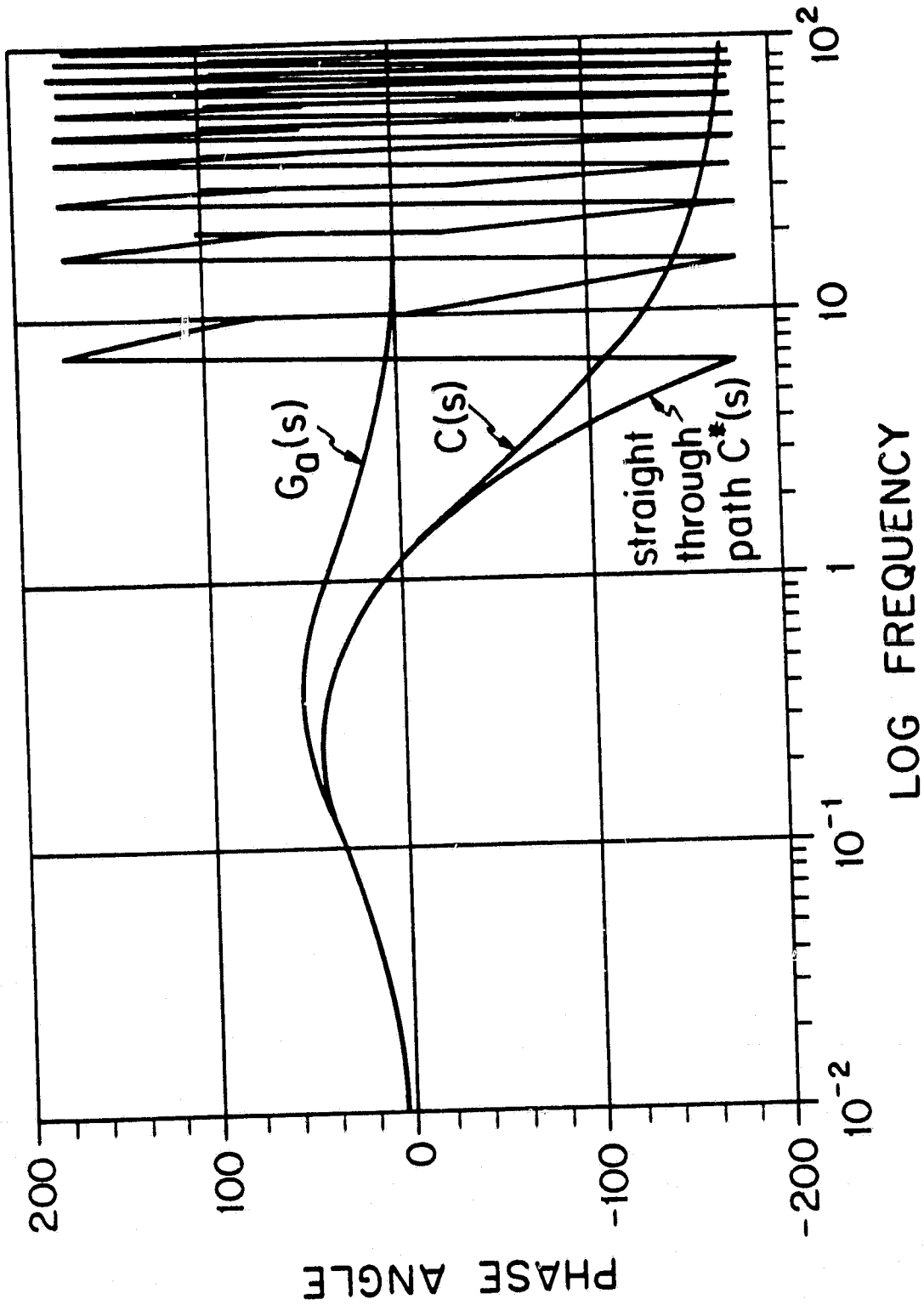FIGURE 9b: Zero-Order-Hold.

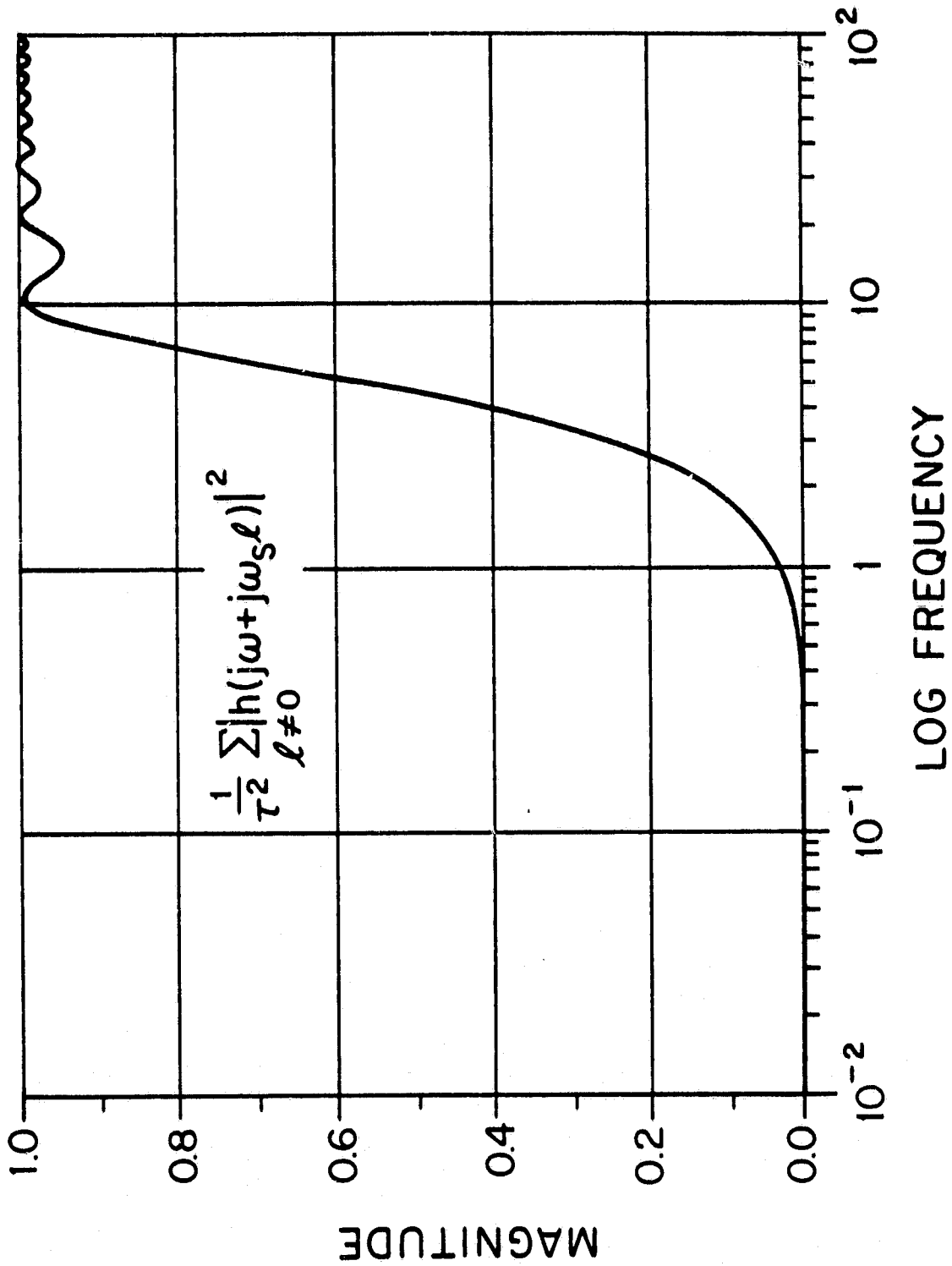FIGURE 10a: Lead Compensator

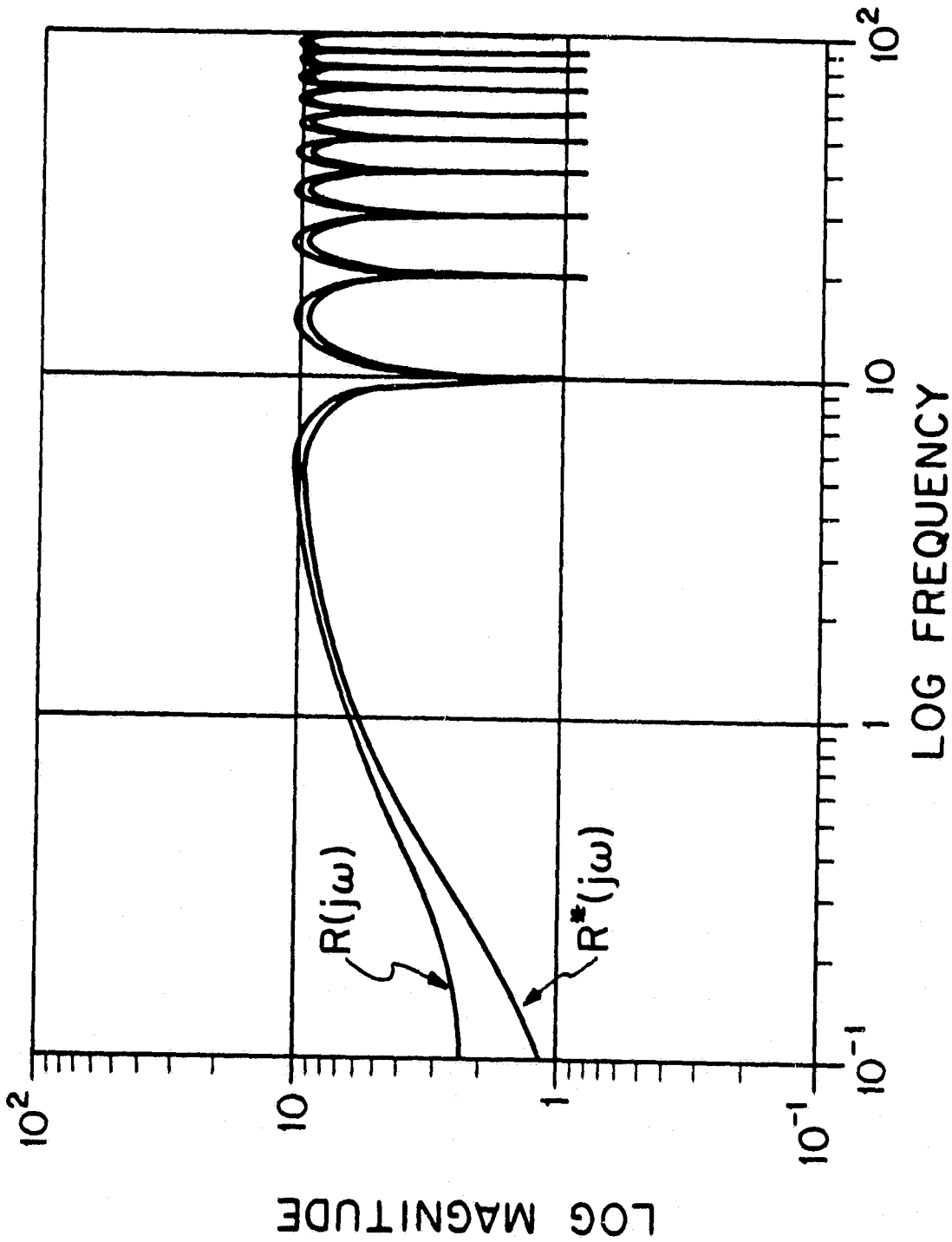FIGURE 10b: Lead Compensator.

FIGURE 11: One Infinite Sum.

FIGURE 12: Sector Radii.

at $\omega=\omega_s = 10$ r/s appears as a DC level in the radius corresponding to $C(s)$. This illustrates that any design advantages offered by a simple cone centers must be paid for with large radii and with the associated more severe stability robustness restrictions and/or performance degradations discussed in Section 3.

Some Basic Tradeoffs

Whether or not a given sector approximation is useful for feedback design depends on the relative magnitude of its radius when compared with the corresponding center. We have already observed this relationship in Section 3. In particular, if a loop transfer operator G is any member of Sector (C, R), then our stability robustness condition (26) required that

$$||R(I+C)^{-1}(\underset{\sim}{c}-\underset{\sim}{d})||_T < ||\underset{\sim}{c}-\underset{\sim}{d}||_T \qquad (66)$$

for all inputs $(\underset{\sim}{c}-\underset{\sim}{d}) \in L_{2e}^m$ and all $T<\infty$

Moreover, to get good performance we required that $(I+C)^{-1}$ be small for some specified subset of inputs, i.e.

$$||(I+C)^{-1}(\underset{\sim}{c}-\underset{\sim}{d})||_T \leq q_o ||\underset{\sim}{c}-\underset{\sim}{d}||_T \qquad (67)$$

for $(\underset{\sim}{c}-\underset{\sim}{d}) \in S$ and all $T<\infty$

If $q_o <<1$, it follows that

$$(I+C)^{-1}(\underset{\sim}{c}-\underset{\sim}{d}) \approx C^{-1}(\underset{\sim}{c}-\underset{\sim}{d}) \qquad (68)$$

and substituting this into (66) we get

$$||R \; C^{-1}(\underset{\sim}{c}-\underset{\sim}{d})||_T < ||\underset{\sim}{c}-\underset{\sim}{d}||_T \tag{69}$$

for all $\underset{\sim}{c}-\underset{\sim}{d} \in S$, all $T < \infty$.

This last expression shows that the sector approximation is useful for feedback design only if its normalized error magnitudes are less than unity for the signal set S. This turns out to be specific statement of a very basic truth in feedback control. We cannot close feedback loops with substantial gain unless the (normalized) loop uncertainties are less than one.

In the example above, of course, we have computed radii and centers not for a complete loop transfer operator but for the hybrid lead compensator alone. A complete loop transfer operator using this compensator will be given by

$$
\begin{aligned}
G_{\text{loop}} &= G \; P \\
&= [C + (G-C)]P
\end{aligned}
\tag{70}
$$

for some plant P and some compensator center C. The normalized loop transfer radius condition (69) then becomes

$$||R_{\text{loop}}C_{\text{loop}}^{-1}(\underset{\sim}{c}-\underset{\sim}{d})||_T = ||RP(CP)^{-1}(\underset{\sim}{c}-\underset{\sim}{d})||_T$$

$$||RC^{-1}(\underset{\sim}{c}-\underset{\sim}{d})||_T < ||\underset{\sim}{c}-\underset{\sim}{d}||_T \tag{71}$$

for all $(\underset{\sim}{c}-\underset{\sim}{d}) \in S$, $T < \infty$

This shows that a sector radius for the compensator alone is also useful for feedback design only if its normalized magnitude is less than unity for the input set S.

As in Section 3, Condition (71) can be interpreted in the frequency domain via

$$\bar{\sigma}[R(j\omega)C(j\omega)^{-1}]<1 \tag{71}'$$

for some frequency range $\omega \leq \omega_o$.

The Sample Rate Tradeoff -- Condition (71)' was evaluated for our second sector approximation of the lead compensator, as defined by (63) and (64). The evaluations were made with several sampling times ranging from $\tau=0.628$ sec ($\omega_s=10$ r/s) to $\tau=0.0628$ sec (100 r/s). Results are plotted in Figure 13. They show that Condition (71)' is not satisfied at any frequency for our baseline value $\tau=0.628$. However, it is satisfied over increasingly larger frequency ranges as τ decreases:

τ	Sampling Rate	Frequency Range
.628 sec	10 r/sec	none
.314	20	0.03 - 5. r/sec
.125	50	0 - 13.
.0628	100	0 - 30.

This result illustrates the dramatic effect that sample rate selection has on digital compensator design. Our hybrid implementation of $G_a(s)$, as modelled by Sector (C,R), does not yield a useful compensator unless
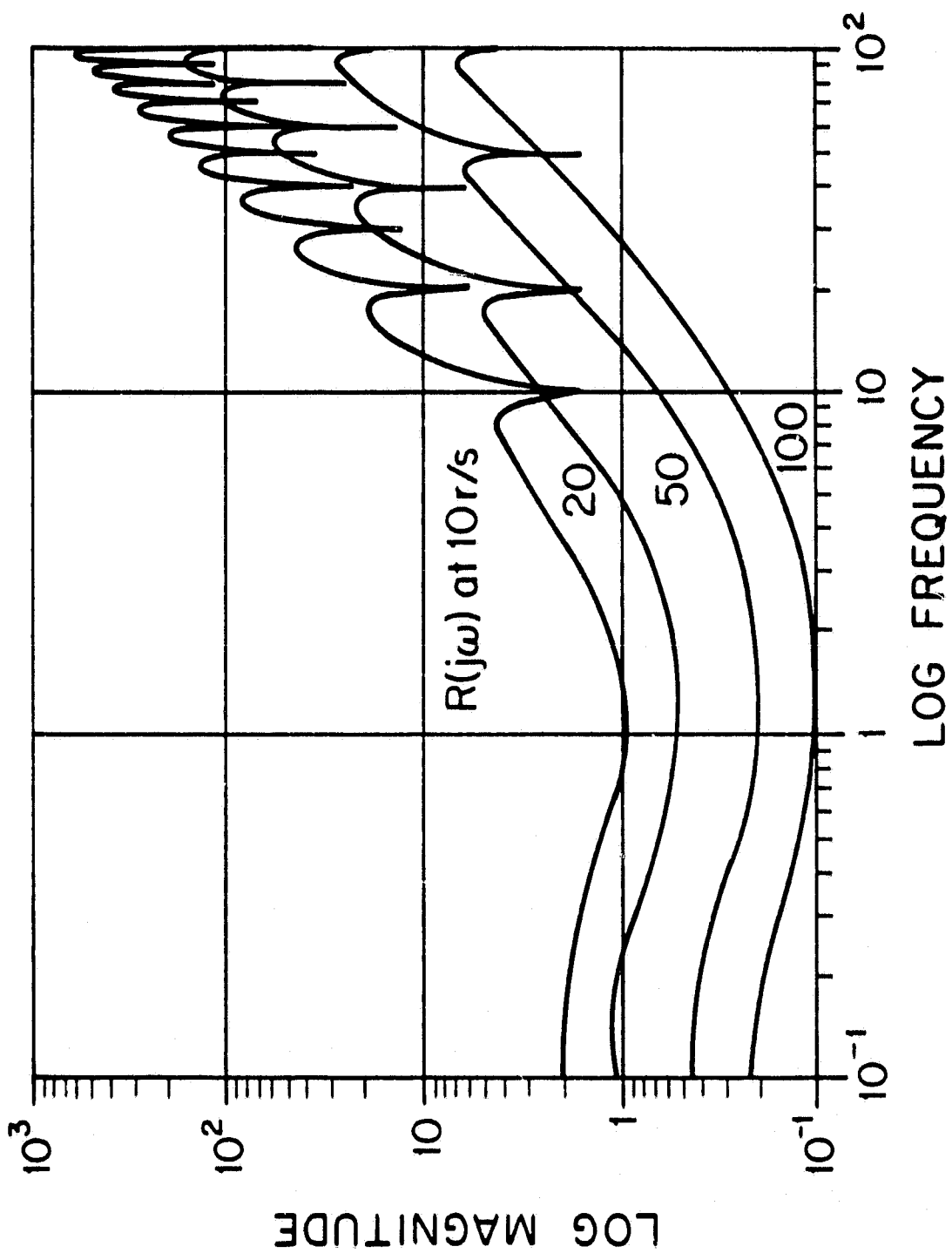
FIGURE 13: Sample Rate Tradeoff.

τ is less than approximately 0.2 seconds. We note that this conclusion is quite consistent with classical "rule of thumb" for selecting sample rates. An old rule due to Stein, for example, is

> "... 5 to 10 samples per radian of the highest
> significant frequency in the control loop..."

In our example, the highest significant frequency is perhaps 1.0 r/s (where the centers C & C* stop developing lead). The resulting rule-of-thumb sample time would therefore be 0.1-0.2 sec.

The Discretization Tradeoff -- In addition to sample time, a second major design parameter in digital implementation is the discretization technique used to convert $G_a(s)$ to $D(z)$. In our results so far, we have used an established pole-zero matching technique as our baseline. Figure 14 compares normalized radii obtained with this technique against the following alternates, all at τ=0.628[12]:

1) the "forward rectangular rule" (replace s in
   $G_a(s)$ by $(z-1)/τ$)

2) the "backward rectangular rule" (replace s in
   $G_a(s)$ by $(z-1)/zτ$)

3) the "Tustin rule" with pre-warping about $ω_1$
   [replace s by $(ω_1/\tan ω_1τ/2)(z-1)/(z+1)$].

The differences between these techniques are seen to be small. None produce a useful sector approximation for the compensator at this sampling time.
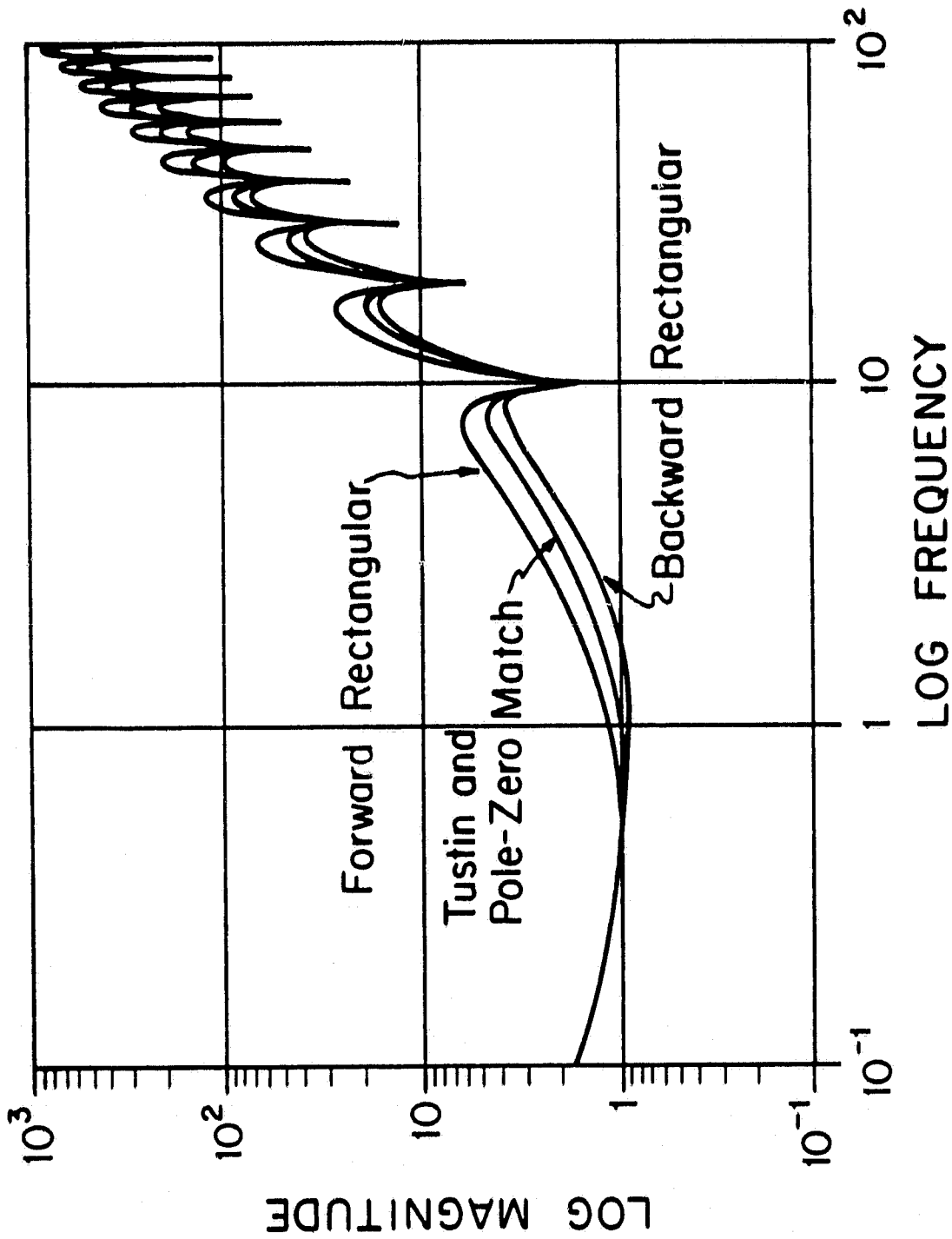
FIGURE 14: Discretization Tradeoff.

We complete our discussion of the lead compensator example at this
point. It is evident that the example and its two simple tradeoffs
above only scratch the surface of the potential utility and range of
application which conic sector concepts offers for digitally implemented
control system design. It is hoped that these results serve to
motivate the needed additional research and design studies.

6. CONCLUSION

This report has presented research results obtained under NASA Grant No. NAG1-2: "Hybrid Operator Models for Digitally-Implemented Control Systems." The results establish a new method of analysis for digitally-implemented (hybrid) control systems based on conic sector concepts from functional analysis. Conic sectors are used to approximate the true complex time-varying nature of a hybrid compensators with a simple time-invariant analog system. The errors of this approximation are rigorously accounted for in the analysis, both in terms of their effect on stability robustness and on performance.

Two specific conic sector approximation were developed for general hybrid systems. One sector produces a conservative non-dynamic radius, while the other is less conservative and frequency dependent. The latter sector has so far been derived only for stable scalar systems. It was illustrated with a simple lead compensator example. This example confirms the computational feasibility of conic sector analysis and also serves to illustrate its potential utility and range of application.

The conic sector concept promises to unify both analog and digital control design techniques under the more general common umbrella of feedback design for systems with approximation errors. Much work remains however to achieve this end. Tighter, less conservative conic sector approximations for general multi-input multi-output hybrid systems remain to be discovered, multi-rate systems remain to be analyzed, and the entire area of efficient numerical algorithms for conic sector analysis remain to be explored.

7. REFERENCES

1. Status Report on "Optimal Design Methods for Multivariable Sample-Data Control Systems," NASA Grant NSG-1312.

2. M. Athans, "The Role and Use of the Stochastic Linear-Quadratic-Gaussian Problem in Control System Design," *IEEE Trans. Auto. Control*, Dec. 1971, pp. 529-551.

3. A.H. Levis, "On the Optimal Sample-Data Control of Linear Processess," Ph.D. Thesis, MIT, June 1968.

4. M.G. Safonov and M. Athans, "Gain and Phase Margins for Multiloop LQG Regulators," *IEEE Trans. Auto. Control*, April 1977.

5. M.G. Safonov, "Robustness Aspects of Stochastic Multivariable Feedback System Design," Ph.D. Thesis, MIT, 1977.

6. A. Kostovetsky, "Some Investigations of Hybrid Systems," M.S. Thesis, Massachusetts Institute of Technology, Dept. of Mech. Eng., May 1979.

7. G. Zames, "On the Input-Output Stability of Time-Varying Nonlinear Feedback Systems, Parts I and II," *IEEE Trans. Auto. Control*, AC-11, pp. 228-238, 465-476, 1966.

8. J.C. Doyle and G. Stein, "Multivariable Feedback Design: Concepts for a Classical/Modern Synthesis," *IEEE Trans. Auto. Control*, AC-26, pp. 75-82, 1981.

9. J.C. Willems, *The Analysis of Feedback Systems*, MIT Press, Cambridge, MA, 1971.

10. N.R. Sandell,Jr., "Robust Stability of Systems with Application to Singular Perturbations," *Automatica*, Vol. 15, pp. 467-470, 1979.

11. C.A. Desoer and M. Vidyasagar, *Feedback Systems: Input-Output Properties*, Academic Press, New York, 1966.

12. G.F. Franklin and J.D. Powell, *Digital Control of Dynamic Systems*, Addison-Wesley, Reading, MA, 1980.

13. N.A Lehtomaki, "Practical Robustness Measures in Multivariable Control Systems Analysis," Ph.D. Thesis, MIT, May 1981.